### Title
Near-infrared study of fluctuations in cerebral hemodynamics during rest and motor stimulation: Temporal analysis and spatial mapping




### Journal
Medical Physics, 27(4)

### ISSN
0094-2405



### Authors
Toronov, Vlad
Franceschini, Maria Angela
Filiaci, Mattia
et al.



### Publication Date
2000-04-01

### DOI
10.1118/1.598943

Medical Physics
The International Journal of Medical Physics Research and Practice

# Near-infrared study of fluctuations in cerebral hemodynamics during rest and motor stimulation: Temporal analysis and spatial mapping

Vlad Toronov, Maria Angela Franceschini, Mattia Filiaci, Sergio Fantini, Martin Wolf, Antonios Michalos, and Enrico Gratton

Citation: Medical Physics **27**, 801 (2000); doi: 10.1118/1.598943
View online: http://dx.doi.org/10.1118/1.598943
View Table of Contents: http://scitation.aip.org/content/aapm/journal/medphys/27/4?ver=pdfcov
Published by the American Association of Physicists in Medicine

# Near-infrared study of fluctuations in cerebral hemodynamics during rest and motor stimulation: Temporal analysis and spatial mapping

Vlad Toronov,[a] Maria Angela Franceschini,[b] Mattia Filiaci, Sergio Fantini,[b] Martin Wolf, Antonios Michalos, and Enrico Gratton
*Laboratory for Fluorescence Dynamics, Department of Physics, University of Illinois at Urbana—Champaign, 1110 West Green Street, Urbana, Illinois 61801-3080*

(Received 13 July 1999; accepted for publication 17 January 2000)

We have noninvasively studied the motor cortex hemodynamics in human subjects under rest and motor stimulation conditions using a multichannel near-infrared tissue spectrometer. Our instrument measures optical maps of the cerebral cortex at two wavelengths (758 and 830 nm), with an acquisition time of 160 ms per map. We obtained optical maps of oxy- and deoxy-hemoglobin concentration changes in terms of amplitudes of folding average, power spectrum and coherence at the stimulation repetition frequency, and the phase synchronization index. Under periodic motor stimulation conditions, we observed coherence and frequency or phase synchronization of the local hemodynamic changes with stimulation. Our main findings are the following: (1) The amplitude of the hemodynamic response to the motor stimulation is comparable to the amplitude of the fluctuations at rest. (2) The spatial patterns of the oxy- and deoxy-hemoglobin responses to the stimulation are different. (3) The hemodynamic response to stimulation shows a spatial localization and a level of phase synchronization with the motor stimulation that depends on the stimulation period.  [S0094-2405(00)00404-1]

Key words: tissue optics, near-infrared spectroscopy, brain physiology

## I. INTRODUCTION

The advantages of near-infrared spectroscopy (NIRS), such as noninvasiveness, high temporal resolution, and relatively low cost, make it an effective method for studying the dynamics of physiological processes, particularly brain hemodynamics.[1] Recent near-infrared measurements of brain activity following visual[2–4] and motor[5–10] stimulations confirmed the positron emission tomography[11] and functional magnetic resonance imaging[12] observations of a significant hemodynamic response at the activated brain area. Several important features of cerebral hemodynamics were discovered. For instance, it was found that while the oxy- and deoxy-hemoglobin concentrations exhibit irregular fluctuations at rest,[13] typically during stimulation the statistical average change of deoxy-hemoglobin concentration in the activated brain area is negative, and the corresponding oxy-hemoglobin change is positive.[1,2,7,9] The dependence of the hemodynamic response on the duration of the relaxation phase preceding a motor stimulation was demonstrated.[10] Because of its high temporal (~10 ms) and good spatial (~mm) resolution, NIRS is particularly advantageous for mapping functional cerebral hemodynamics. A number of near-infrared instruments for mapping cerebral hemodynamics by simultaneous multisite probing were described in the literature.[14–16] The results of the multisite monitoring of cerebral hemodynamics during mental tasks were described in Ref. 17. However, in most articles presenting optical maps of brain activity[7,8] the measurements were performed with one source–detector channel by repeating the stimulation protocol sequentially at each measurement position, resulting in a slow acquisition time per image (40–60 min). Only Ref. 9 presents optical maps of a cerebral hemodynamic response to motor stimulation obtained by a multichannel instrument with the acquisition time of 1–2 s per image.

In this article we discuss temporal and spatial patterns of brain hemodynamics under rest and motor stimulation conditions obtained by fast (160 ms per image) multisite NIRS measurements in the motor cortex area. Particularly, we study the relationship between underlying hemodynamic fluctuations and responses to stimulation. Our near-infrared instrument allows noninvasive data acquisition from eight sources and two detectors on the human head. The measurements were performed on a group of five healthy male subjects. To study the hemodynamics dependence on the motor task timing, we follow a measurement protocol that includes a number of rest and finger-motion exercise epochs. The exercise epochs consist of the repetition of stimulation/relaxation cycles. The relative duration of stimulation and relaxation is different for different epochs.

To assess statistical properties of cerebral hemodynamics and to generate optical maps of brain activity, we employ a combination of different statistical methods for the analysis of NIRS data. The reason for using a variety of methods is the complex character of the hemoglobin concentration temporal patterns both under stimulation conditions and at rest.[13] In addition to statistical tests of significance of hemodynamic changes and folding average analysis, the traditional methods of time series statistical analysis are the power spectrum and coherence analyses based on the Fourier transform.[13] Recently a new time-domain method of data analysis was developed, which allows the detection and quantification of phase synchronization between two signals.[19] This method

was successfully applied to the analysis of synchronization between the magnetoencephalograms and records of muscle activity in a Parkinsonian patient. The phase synchronization analysis is important because, as shown in Ref. 19, phase synchronization is not equivalent to coherence or frequency synchronization, being an independent characteristic of the interrelationship between two processes. We compare dynamic features and optical maps of hemodynamic signals obtained using different data analysis techniques, including both the traditional folding average and Fourier transform methods, as well as the new quantitative phase synchronization analysis. We also discuss the validity of different tests, such as Student *t* test, sign test,[20] and Wilcoxon matched-pair signed-rank test,[20] for the assessment of statistical significance of the cerebral hemodynamic changes under the motor stimulation conditions.

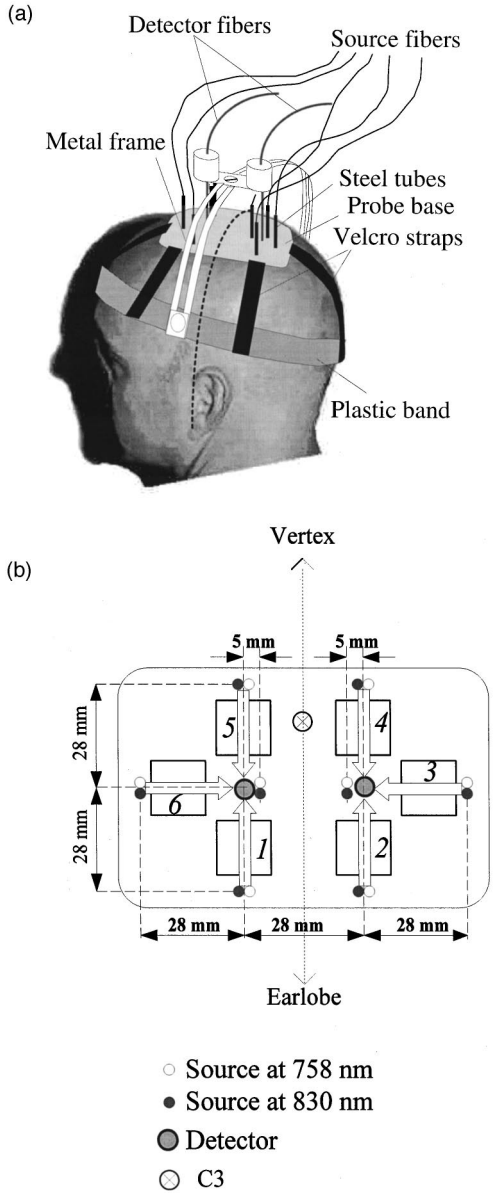


FIG. 1. (a) The headset for holding the fiber-optic probe designed for measurements on the motor cortex. The broken line shows the vertex-earlobe line. (b) Geometric arrangement of the optical fibers in the probe. The crossed circle marks the hole in the probe pad that was matched with the measured C3 position on the subject's head. The arrows show six 28 mm source–detector channels corresponding to the square zones *1–6* in the optical maps. The dashed vertex-earlobe line shows the orientation of the probe on the head.

## II. INSTRUMENTATION AND METHODS

### A. Near-infrared optical system and medical monitoring equipment

We use a two-wavelength instrument for near-infrared probing of tissues in which light emitted by laser diodes (758 and 830 nm, ~2 mW average power) is guided to the tissue through multimode silica optical fibers (400 $\mu$m core diameter). Sixteen laser diodes (eight per each wavelength) operate in a sequential multiplexing mode with 10 ms on time for each diode. Two glass fiber bundles (3.2 mm internal diameter) collect the scattered light and conduct it to the photomultiplier tube (PMT) detectors. The 16 sources and 2 detectors provide 32 source–detector channels. The output signals from the PMTs are applied to the inputs of an interface card for an IBM-PC computer, where data processing is performed. To obtain cerebral optical maps, we designed a headset [see Fig. 1(a)] consisting of the fiber-optic probe [Fig. 1(b)] and a frame securing the probe on the head. Two detector fibers are securely fixed in the central part of the probe [see Fig. 1(b) for distances]. The paired (758 and 830 nm wavelength) source optodes are attached to the probe pad at eight positions. The range of source–detector distances allows us to distinguish processes occurring at different tissue depths. To probe the superficial tissue layer, we use two 0.5 cm source–detector channels. For brain mapping we use six equidistant 2.8 cm channels denoted by italic numbers *1–6* in Fig. 1(b) and throughout the text.

In addition to the optical signals probing the brain hemodynamics, we acquire the heart rate and the arterial saturation by means of a pulse oximeter N-200 (Nellcor) with the sensor attached to the left-hand index finger, and the respiratory signal with the monitoring system Resp-EZ (Sleepmate/Newlife Technologies). All these physiological signals are acquired by the PC computer simultaneously with the near-infrared signals.

### B. Motor stimulation protocol: a stimulation wave

We performed measurements on five subjects: right-handed males of age ranging from 30 to 65 years. A written informed consent was obtained from each subject before measurements. The subjects had very short blond hair, or very rare hair of arbitrary color, or were hairless. The probe was positioned on the left side of the head in such a way that the point shown in Fig. 1(b) with the cross mark coincided with the measured middle point (C3 position) of primary motor cortex. This point was found as the one that marks 40% of the distance from the vertex to the left earlobe on the line connecting the vertex and the left earlobe.[21]

During measurements the subjects were comfortably supine and instructed not to speak or to make unnecessary movements. Each measurement consisted of the rest epoch (10 min) and three to four exercise epochs. During the rest epoch, the baseline data were acquired. During the exercise epoch, subjects were asked to begin or stop performing a finger motion (a light palm squeezing) exercise by the right hand. The squeezing rhythm (1.5 Hz) was maintained by means of a metronome. Three subjects performed three exercise epochs E1, E2, and E3 differed by the duration of the stimulation/relaxation period: 20/60, 20/20, 10/17 s, respectively, and consisted of 5, 10, and 10 periods, respectively. Two other subjects performed four exercises, including the same E1, E2, and E3, and one more consisting of ten 10/10 s stimulation/relaxation periods.

Mathematically each exercise epoch can be associated with a rectangular stimulation wave, whose magnitude is zero during relaxation phases and one during stimulation phases. We used such stimulation rectangular waves in the analysis of coherence and phase synchronization between the stimulation and hemoglobin signals.

### C. Reconstruction of hemodynamics from optical data

To convert optical intensity data into hemodynamic concentration changes, we assume a model for light transport in strongly scattering medium based on the diffusion approximation to the Boltzmann transport equation,[22] and that the absorption variations in the tissue are only due to oxy- and deoxy-hemoglobin. The diffusion model of light transport gives the following equation to compute the change in the absorption coefficient $\Delta\mu_a^{\lambda}$ at a given wavelength between its values corresponding to the initial intensity $I_{\lambda 0}$ and intensity $I_{\lambda}$:

$$\Delta\mu_a^{\lambda} = -\frac{\ln(I_{\lambda}/I_{\lambda 0})}{d\sigma_{\lambda}}, \tag{1}$$

where $d$ is the distance between the source and the detector fibers, and $\sigma_{\lambda}$ is the differential pathlength factor (DPF). We use the adult head DPF values of 6.2 at $\lambda_1 = 758$ nm and 5.9 at $\lambda_2 = 830$ nm according to Ref. 23. Changes of $[\mathrm{HbO_2}]$ and [Hb] corresponding to the changes in the absorption coefficients $\Delta\mu_a^{\lambda 1,2}$ of the tissue at the wavelengths $\lambda_1$ and $\lambda_2$ can be obtained using the equations[24]

$$\Delta[\mathrm{HbO_2}] = \frac{\Delta\mu_a^{\lambda 1}\epsilon_{\mathrm{Hb}}^{\lambda 2} - \Delta\mu_a^{\lambda 2}\epsilon_{\mathrm{Hb}}^{\lambda 1}}{\epsilon_{\mathrm{HbO_2}}^{\lambda 1}\epsilon_{\mathrm{Hb}}^{\lambda 2} - \epsilon_{\mathrm{Hb}}^{\lambda 1}\epsilon_{\mathrm{HbO_2}}^{\lambda 2}}, \tag{2}$$

$$\Delta[\mathrm{Hb}] = \frac{\Delta\mu_a^{\lambda 2}\epsilon_{\mathrm{HbO_2}}^{\lambda 1} - \Delta\mu_a^{\lambda 1}\epsilon_{\mathrm{HbO_2}}^{\lambda 1}}{\epsilon_{\mathrm{HbO_2}}^{\lambda 1}\epsilon_{\mathrm{Hb}}^{\lambda 2} - \epsilon_{\mathrm{Hb}}^{\lambda 1}\epsilon_{\mathrm{HbO_2}}^{\lambda 2}}. \tag{3}$$

Here $\epsilon_{\mathrm{Hb}}^{\lambda 1,2}$ and $\epsilon_{\mathrm{HbO_2}}^{\lambda 1,2}$ are the extinction coefficients of Hb and $\mathrm{HbO_2}$, respectively, at wavelengths $\lambda_1$ and $\lambda_2$ (values may be found in Ref. 25).

Equations (1), (2), and (3) are derived assuming the homogeneity of the scattering medium, and therefore they are not expected to provide accurate quantitative intracranial hemodynamics assessment. In Ref. 26 it was argued that light propagation in the adult head is highly affected by the clear cerebrospinal fluid (CSF). On the basis of a computer model, Okada *et al.* found that at source–detector separations greater than 3 cm the detected light passes mainly through the CSF layer, and the optically probed brain region is confined to a shallow portion of the gray matter. At a source–detector distance of 3 cm, the contribution of the gray matter to the light absorption is in the order of 20%–30%. Even though these results are based on assumed optical properties of the involved tissue layers whose accuracy is not known, there is some indication that it may be difficult for NIRS to quantify intacranial changes of $[\mathrm{HbO_2}]$ and [Hb]. Therefore, in this article we do not aim at quantifying the absolute hemodynamic changes in the motor cortex, but rather we aim at the analysis of temporal characteristics and relative changes in different regions of the cortex.

Since we assess hemoglobin concentration changes in different zones of the motor cortex, the notations for the hemoglobin concentration change throughout the text include the zone number denoted by the italic subscript. For example, $[\mathrm{Hb}]_3$ denotes the deoxy-hemoglobin change in zone *3* according to Fig. 1(b).

### D. Statistical tests of significance of hemodynamic changes

To detect brain responses to motor stimulation, we tested statistical significance of hemoglobin concentration changes between the stimulation and relaxation phases. The compared values were the [Hb] changes from its value at the beginning of the cycle averaged for the last 10 s of the stimulation period and for the last 10 s of the entire cycle. The beginning of the cycle was chosen in the middle of the relaxation period. We defined the significance level equal to the common value of 0.05, i.e., the hemodynamic changes are significant if the test probability $p \leqslant 0.05$.

Since the number of samples for each epoch was small (equal to the number of stimulation cycles), the normality of the distributions could not be tested with a high confidence, and the use of the Student *t* test was not justified. When the type of the distribution is uncertain, the most robust test is the sign test,[20] which analyzes the signs of the differences between the pairs of compared values. The sign test answers the following question: ''Does the decrease of [Hb] (or the increase of $[\mathrm{HbO_2}]$) during the stimulation occur often enough to be significant?,'' but the result of the test does not depend on the magnitude of the change.

Another appropriate test is the Wilcoxon matched-pair signed-rank test. This test uses not only the signs of the changes,but also their magnitudes. For small numbers of samples with unknown distributions, the Wilcoxon test is more sensitive than the Student *t* test.[20] The basic assumption of the Wilcoxon test is that the distribution of the difference between the values within each pair must be symmetric,

which is less restrictive than the *t*-test assumption of the normality of pair member distributions.

### E. Folding average

Assuming synchronization between stimulation and hemoglobin response, one can separate the response from fluctuations by means of a folding average. This procedure includes algebraic averaging of data corresponding to the same point on the stimulation/relaxation cycle over a number of cycles and returns the averaged signal evolution during the period of stimulation/relaxation. The beginning of the cycle was chosen in the middle of the relaxation period. Before calculating folding averages, we performed a linear detrending of the data on each folded period for additional fluctuation suppression. In the optical maps of brain signals (see Sec. II H) we plot the magnitude of the folding average hemoglobin concentration change, which we defined for $[HbO_2]$ as the difference between the maximum and minimum folding-average values, and for [Hb] as the difference between the minimum and maximum values.

### F. Power spectrum and coherence

We analyzed the autocorrelation power spectra of the oxy- and deoxy-hemoglobin signals, and the spectra of coherence between the stimulation rectangular wave defined in Sec. II B and the hemoglobin signal. The autocorrelation power spectrum $P_k(\nu)=\langle|f_k(\nu)|^2\rangle$ of the data series (for example, of $[Hb]_k$ or $[HbO_2]_k$ series, where $k$ is the light channel) at frequency $\nu$ can be obtained by averaging the squared magnitudes of complex Fourier transforms $f_k(\nu)$ of successive (possibly overlapping) data subsets.[18] The inverse Fourier transform of $P_k(\nu)$ returns the autocorrelation function.[18] The coherence spectrum[18] of two data series (labeled with indices $k$ and $m$) is defined as the normalized average product of the corresponding complex Fourier transforms $C_{km}(\nu)=\langle f_k(\nu)f_m^*(\nu)\rangle/\sqrt{P_k(\nu)P_m(\nu)}$. Note that $C_{km}(\nu)$ is a complex function of $\nu$. The normalization to the square root of the product of the autocorrelation power spectra restricts the absolute values of $C_{km}(\nu)$ to the interval between 0 and 1. $|C_{km}(\nu)|$ approaches 1 when there is a high correlation between two processes at the given frequency $\nu$, particularly when the two series are identical, and it approaches zero when there is no statistical correlation between the two processes at the given frequency. The phase of $C_{km}(\nu)$ may be interpreted as the average phase difference between the two signals at frequency $\nu$.

To compute $f_k(\nu)$ for a discrete set of frequency values $\nu$ we use the fast Fourier transform algorithm. The bandwidth and the frequency resolution of the autocorrelation and coherence spectra are determined by the sampling rate and by the length of the data subset, respectively. For the measurements reported in this work the acquisition time per point is 160 ms, which corresponds to a frequency bandwidth of 3.125 Hz. The duration of each subset data trace to produce a Fourier transform is 164 s, which corresponds to a spectral resolution of 0.0061 Hz.

### G. Phase synchronization

We estimated the phase synchronization strength between the stimulation rectangular wave and the oxy- and deoxy-hemoglobin signals. According to the definition,[19] two periodic quasiharmonic signals having phases $\phi_1(t)$ and $\phi_2(t)$ (defined on the infinite interval) are phase locked, or phase synchronized if there are two integer numbers $n$ and $m$ such that $|n\phi_1(t)-m\phi_2(t)|<\text{const}$. For periodic, quasiharmonic signals the phase synchronization condition is equivalent to the frequency locking condition $n\omega_1=m\omega_2$, since for periodic oscillators $\omega_k=\overline{\dot{\phi}_k}(t)$ (where the overbar denotes the time average). Recently, phase synchronization was understood as a specific relationship between two signals of arbitrary nature, including nonperiodic and noisy signals.[19] This interpretation required a generalization of the concept of phase and of the mathematical condition restricting the relative phase change of two signals. For an arbitrary real function of time, $F(t)$, the phase may be defined as the phase of the complex analytical continuation of the given function into the complex plane.[18] The real part of this analytical function is given by the original function $F(t)$, and the imaginary part $Q(t)$ is given by the Hilbert transform of $F(t)$:

$$Q(t)=\int_{-\infty}^{\infty}\frac{F(u)}{\pi(t-u)}du. \tag{4}$$

The condition $|n\phi_1(t)-m\phi_2(t)|<\text{const}$, where $\phi_{1,2}(t)$ are the phases of analytical continuations of two signals taking their values on the interval $(-\infty, \infty)$, may still be considered as a phase-locking condition. However, as it was shown in Ref. 19, in the case of noisy signals this condition may not be always fulfilled. Instead, the authors of Ref. 19 proposed a definition of phase synchronization that assumes a statistical quantification of the synchronization strength. The basis of this quantification is as follows. (i) One should identify two integers $n$ and $m$ such that the relative phase $\Psi_{nm}=n\phi_1(t)-m\phi_2(t)$ [defined on the interval $(-\infty, \infty)$] fluctuates over horizontal plateaus separated by jumps exceeding $2\pi$ in amplitude. The horizontal plateaus correspond to those time intervals when there is a phase synchronization between two signals, and the jumps occur when the synchronization is lost. The reduction of the relative phase $\Psi_{nm}$ to the phase $\breve{\psi}_{nm}$ defined on the interval $(-\pi, \pi)$ brings the horizontal plateaus approximately to the same level, if the jump magnitudes are close to integer multiples of $2\pi$. (ii) The sharpness of the probability distribution of the reduced phase $\breve{\psi}_{nm}$ over the interval $(-\pi, \pi)$ characterizes the strength of phase synchronization. The sharpness of the probability distribution $P_i$ over $N$ bins can be quantified by the Shannon entropy $S=-\Sigma_{i=1}^{N}P_i\,\text{Ln}(P_i)$. A uniform distribution has the entropy value $S_{\max}=\text{Ln}(N)$. (iii) To characterize the deviation of the distribution from the uniformity, one can use the *index* $\eta=(S_{\max}-S)/S_{\max}$. It is this index $\eta_{nm}$ calculated for the distribution of $\breve{\psi}_{nm}$ over the interval $(-\pi, \pi)$ that is the entropy

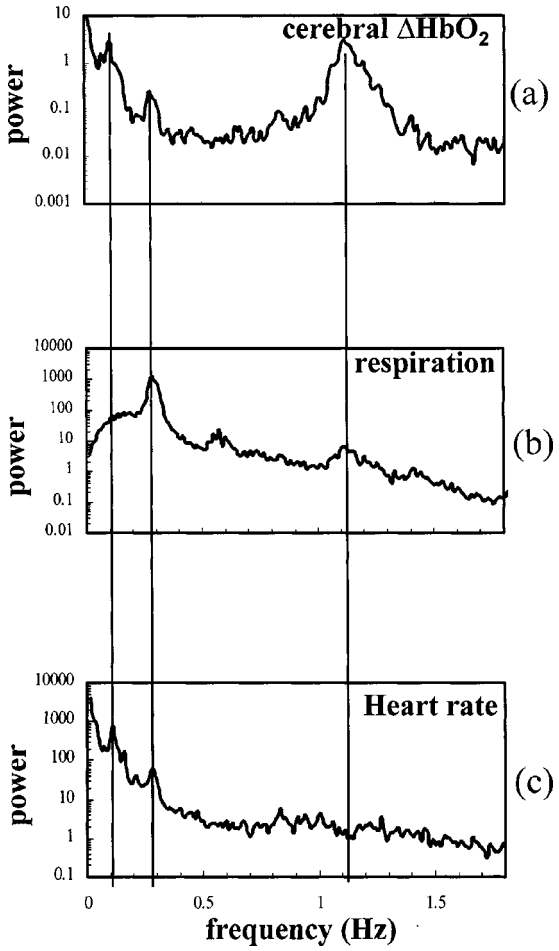


FIG. 2. Power spectra of (a) $[HbO_2]$, (b) respiration signal, and (c) heart-rate variability signal acquired simultaneously on a 34-year-old healthy right-handed male at rest conditions. The vertical lines show the alignment of the spectral peaks.

phase synchronization index (PSI) that was proposed in Ref. 19 to quantify the strength of the $(n:m)$ phase synchronization state.

It is important to note that in the case of strong $(n:m)$-phase synchronization characterized by the integer numbers $n$ and $m$, there is also a strong $(n:m)$-frequency locking in terms of the sharpness of the distribution for the function $\Omega_{nm}=n\omega_1(t)-m\omega_2(t)$, where $\omega_k(t)=\dot{\phi}_k(t)$ are the instantaneous frequencies and $\phi_k(t)$ are the phases of the complex analytical signals. However, this statement may not be generally inverted. In other words, frequency synchronization may indicate phase synchronization, but is not equivalent to it. Thus, two signals may be frequency locked, but not phase synchronized. Furthermore, as it was shown in Ref. 19, the (1:1)-phase synchronization between two signals is not equivalent to their coherence: the signals may be coherent, but not phase locked.

In practice, to detect and measure the degree of phase synchronization one should try different pairs of integer numbers $n$ and $m$ to find the pair that gives the maximal value of $\eta_{nm}$. Note that since $\eta_{nm}$ measures the deviation of a given distribution of $\breve{\psi}_{nm}$ values from the uniform distribution, any two finite datasets exhibit some nonzero PSI values. Therefore, to avoid spurious detection of synchronization between two signals represented by the time series of the length $L$, one should disregard $\eta_{nm}$ values that are below the significance level determined by the statistical distribution of PSI values corresponding to all possible $L$-length sets of random data having a homogeneous distribution on the interval $(-\pi, \pi)$ in the limit $L\to\infty$.

To calculate PSI, we filtered the time series using a nonrecursive digital filter[27] having a pass band centered at the repetition frequency of stimulations, heart rate, or breathing rate. Then we performed the numerical Hilbert transform[18] of filtered signals to obtain imaginary parts of the corresponding complex analytical signals. After that, the reduced relative phase $\breve{\psi}_{nm}(t)$ calculated from the phases of analytical signals was analyzed statistically to obtain PSI values. Only significant values were considered. We assumed the significance level to be equal to the mean plus one standard deviation of the PSI value distribution for all possible equiprobable random datasets of the same length as the analyzed one.

### H. Generation of optical maps

We used values resulting from the folding average, power spectrum, coherence spectrum, and phase synchronization analyses for mapping brain motor activity. The optical maps are made of six pixels corresponding to the squares labeled as *1–6* in Fig. 1(b). The value of each pixel was obtained using data from the corresponding 2.8 cm source–detector pair. The six pixels of an optical map correspond to six zones in the motor cortex area.

## III. TEMPORAL ANALYSIS

### A. Spontaneous fluctuations under rest conditions

Optical signals acquired on the head under rest conditions exhibit fluctuations. Figure 2(a) shows an $[HbO_2]$ fluctuation power spectrum in the frequency range between 0.01 and 1.8 Hz as obtained by NIRS on a 34-year old healthy right-handed male at rest conditions in the area of a motor cortex [zone 5 according to Fig. 1(b)]. The source–detector separation is 2.8 cm. A typical $[HbO_2]$ power spectrum, as the one shown in Fig. 2(a), includes a heartbeat peak and the structures towering around the average respiration frequency and some frequency lower than the respiratory one, which for the given subject are at about 1.1, 0.3, and 0.1 Hz, respectively. One can identify the respiratory structure in the $[HbO_2]$ spectrum by comparison with the power spectrum of the respiratory monitor signal [Fig. 2(b)] acquired simultaneously with the spectrum shown in Fig. 2(a). Respiratory oscillations in the NIRS signals were also described in Ref. 28. Note that the power spectrum of the pulse oximeter heart-rate signal [Fig. 2(c)] shows peaks both at the respiratory frequency (due to the sinus arrhythmia) and the lower-frequency peak of the $[HbO_2]$ spectrum ($\sim$0.1 Hz). Therefore, one can believe that the heart-rate variability is the factor contributing to the $[HbO_2]$ spectrum below 0.5 Hz at

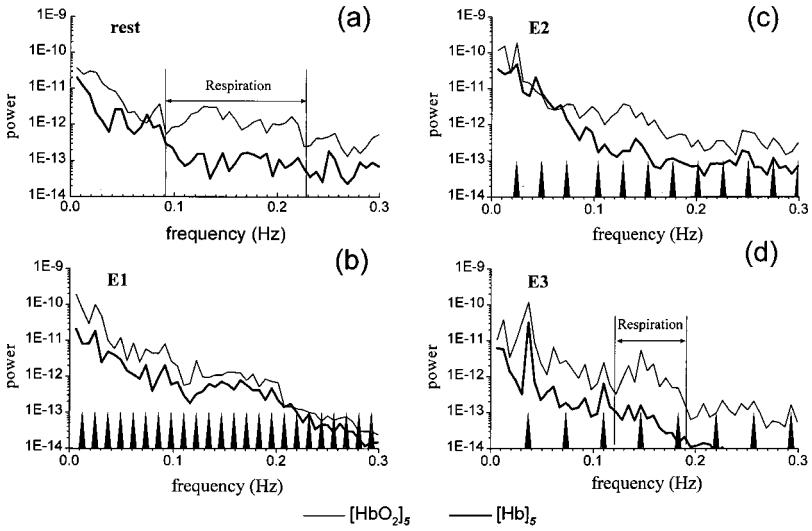


FIG. 3. $[Hb]_5$ and $[HbO_2]_5$ power spectra obtained at rest (a) and during three exercise epochs E1 (20/60 s), E2 (20/20 s), and E3 (10/17 s) (b)–(d). The data [see Figs. 4(a)–(d)] were acquired on one subject (43-year-old healthy right-handed male). The order of figures [(a)–(d)] corresponds to the order of the epoch sequence. The wedge-shaped markers in (b), (c), and (d) indicate the harmonics of the stimulation repetition frequency.

rest. In the [Hb] spectrum (not shown in Fig. 2), the corresponding structures are much less pronounced than in the $[HbO_2]$ spectrum.

In different subjects the average breathing frequency varies approximately between 0.1 and 0.4 Hz. Besides the sinus arrhythmia, the heart-rate variability may exhibit slow changes in the range of 0.01–0.1 Hz. The width of the corresponding spectral peaks varies depending on the regularity of the heart-rate variations and respiration. Figure 3 represents the $[HbO_2]$ and [Hb] fluctuation power spectra acquired on a 43-year healthy right-handed male [zone 5 according to Fig. 1(b), source–detector separation is 2.8 cm] in a more expanded frequency band (0.006–0.3 Hz) than the one of Fig. 2. The corresponding time traces are shown in Fig. 4. The oscillations of frequencies above 0.3 Hz, including the heart beat, are low-pass filtered out and do not appear in Figs. 3 and 4. In the given subject the respiratory oscillations at rest conditions are presented in the $[HbO_2]$ power spectrum [Fig. 3(a)] by the diffuse structure spread between 0.09 and 0.23 Hz. Although the actual period of respiration wave in the $[HbO_2]$ time trace [Fig. 4(a)] varies between 5 and 8 s (0.2 and 0.125 Hz, respectively), the corresponding spectral structure is broadened by the amplitude and frequency modulation of the respiratory wave.

Besides the respiratory fluctuations, both $[HbO_2]$ and [Hb] spectra in Fig. 3(a) show fluctuations in the frequency range below 0.09 Hz (time scales longer than 11 s). Among them the most prominent are the $[HbO_2]$ fluctuations with the peak at about 0.02 Hz corresponding to the 50–60 s time scale in Fig. 4(a). These slow changes correlate with the heart-rate variations observed with the pulse oximeter. In Fig. 3(a) one can also see the peak in the [Hb] power spectrum at about 0.05 Hz, which corresponds to the changes occurring on a time of approximately 20 s. Since this time scale is different from the heart and breathing rates, these 20 s fluctuations may be due to the local spontaneous blood flow fluctuations.

Hemodynamic fluctuations in different zones of a motor cortex at rest conditions are not identical [compare Figs. 4(a) and 5(a) showing rest hemodynamics in the precentral and postcentral areas of the motor cortex]. However, their fluctuation power spectra in the band below 0.3 Hz have similar shapes and magnitudes.

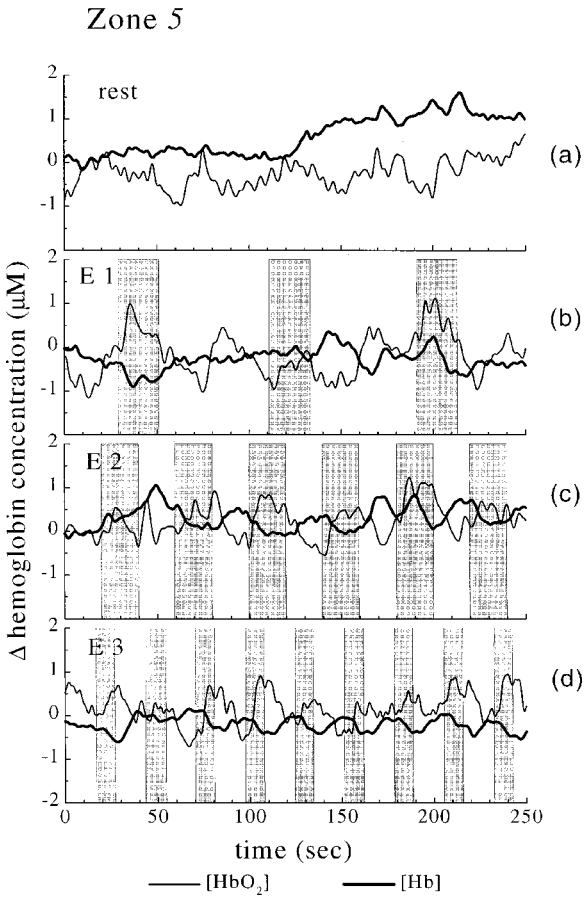


FIG. 4. From (a) to (d): time traces of the oxy- and deoxy-hemoglobin signals corresponding to power spectra shown in (a)–(d), respectively. The order of figures (a)–(d) corresponds to the order of the epoch sequence. The shaded areas indicate stimulation periods. The fluctuations over 0.3 Hz are low-pass filtered out.

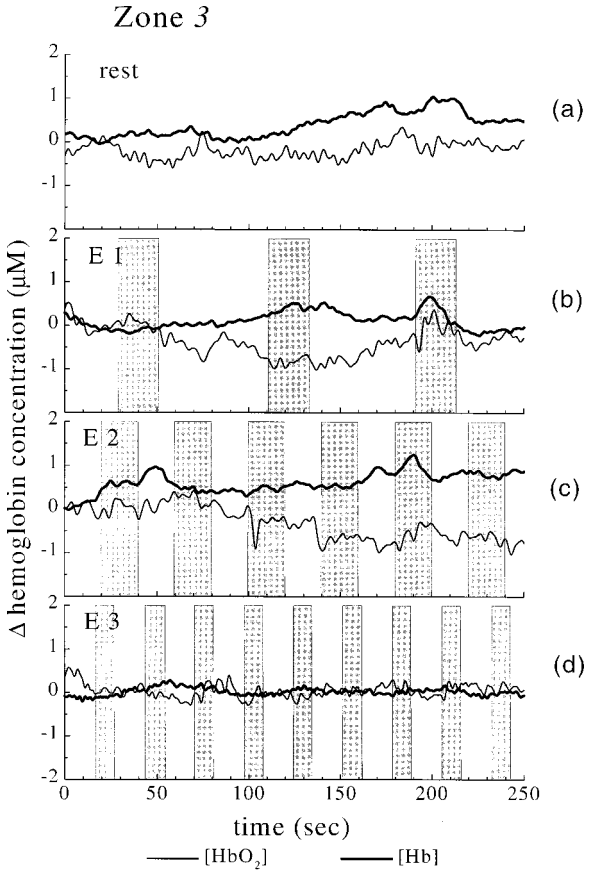


FIG. 5. [Hb] and [$HbO_2$] time traces observed at rest (a) and during three exercise epochs E1 (20/60 s), E2 (20/20 s), and E3 (10/17 s) (b)–(d). The data were acquired at zone 3 on the same subject at the same time as in Fig. 4. The order of figures (a)–(d) corresponds to the order of the epoch sequence. The shaded areas indicate stimulation periods. The fluctuations over 0.3 Hz are low-pass filtered out.

### B. Temporal and spectral patterns of hemoglobin fluctuations during exercises

Figures 3(b)–3(d) and 4(b)–4(d) show power spectra and time traces, respectively, for signals $[Hb]_5$ and $[HbO_2]_5$ (supposedly at the precentral area of the motor cortex), observed in a typical experiment performed according to the protocol described in Sec. II B. The data were acquired during three exercise epochs E1, E2, and E3 differing in the duration of stimulation/relaxation phases (20/60, 20/20, and 10/17 s, respectively). The order of Figs. 3 and 4 corresponds to the actual order of the epoch sequence. The wedge-shaped markers in Fig. 3 show the harmonics of the stimulation repetition frequency. In Fig. 4 the stimulation periods are indicated by the shaded areas.

In Figs. 3 one can see that during epoch E3 [10/17 s stimulation/relaxation period, Fig. 3(d)] both $[Hb]_5$ and $[HbO_2]_5$ power spectra exhibit most sharp peaks at the exercise fundamental frequency and some of its harmonics. For this epoch Figs. 4 show the most regular and synchronous with the stimulation signal $[Hb]_5$ [Fig. 4(d)]. The dynamic pattern of hemoglobin concentration change during E3 is in agreement with the one obtained by other researchers[5–10] by a folding average of the stimulation periods. Namely, in Fig. 4(d) one can clearly see that during the stimulation $[HbO_2]_5$ increases and $[Hb]_5$ decreases, and during the relaxation there is a recovery toward the baseline level.

During epoch E1 (20/60 s), unlike epoch E3, the $[Hb]_5$ time trace does not manifest significant correlation with the stimulation sequence [Fig. 4(b)]. The power spectrum of the $[Hb]_5$ signal has peaks neither at the fundamental frequency nor at the second harmonic [Fig. 3(b)]. The $[HbO_2]_5$ power spectrum has the highest peak at the second harmonic of the stimulation repetition frequency.

During epoch E2 (20/20 s) both $[Hb]_5$ and $[HbO_2]_5$ spectra have peaks at the exercise fundamental frequency and some of its harmonics. The character of the $[Hb]_5$ time trace [Fig. 4(c)] is intermediate between the ones corresponding to the epochs E1 and E3. Indeed, one can recognize a pattern that correlates with the stimulation sequence, but its periodicity is less regular than in the case of the epoch E3. Meanwhile, $[HbO_2]_5$ [Fig. 4(c)] exhibits a quite regular oscillatory pattern.

Figures 5(a)–5(c) show changes in the postcentral area of the motor cortex occurring simultaneously with the changes in the precentral area shown in Figs. 4(a)–4(d). The shaded areas indicate periods of stimulation. One can see that during epochs E1 and E2 [Figs. 5(a) and 5(b), respectively], both the $[Hb]_3$ and $[HbO_2]_3$ changes do not exhibit correlation with the stimulation and are similar to the ones observed at rest [Fig. 5(a)]. During epoch E3 [Fig. 5(d)] no correlation is seen as well, and the amplitude of fluctuations in $[Hb]_3$ and $[HbO_2]_3$ signals are significantly reduced compared to the epochs E1 and E2.

Although the time traces presented in Fig. 4(b) do not manifest clear correlation with the stimulation wave, statistical analysis reveals such a correlation. Because of the small number of samples, we performed the sign test and the Wilcoxon matched-pair signed-rank test of significance for [Hb] changes between stimulation and relaxation phases during epoch E1. The matched pairs were the [Hb] changes from its value at the beginning of the cycle averaged for the last 10 s of the stimulation period and for the last 10 s of the cycle. The beginning of the cycle was chosen to be in the middle of the relaxation period, 30 s before stimulation. To increase the number of samples we tested the common dataset from the zones *1*, *5*, and *6*, which exhibit significant oxyhemoglobin changes during all exercise epochs, and significant deoxyhemoglobin changes during E2 and E3. The test revealed insignificance of the $[Hb]_5$ changes during E1 ($P \leqslant 0.21$). Supposing that this insignificance is due to the interference with the systemic changes, we subtracted the $[Hb]_3$ time series from the $[Hb]_1$, $[Hb]_5$, and $[Hb]_6$ those. After this was done, the Wilcoxon matched pair test has shown the significance ($P \leqslant 0.035$) of the [Hb] changes between stimulation and relaxation during epoch E1. However, the sign test still indicated no significance ($P \leqslant 0.2$), apparently because of the small number of samples (15).

Figure 6 shows the result of the folding average of the $[Hb]_5$ and $[HbO_2]_5$ traces over exercise stimulation/relaxation periods for epochs E1, E2, and E3 [Figs. 6(a),

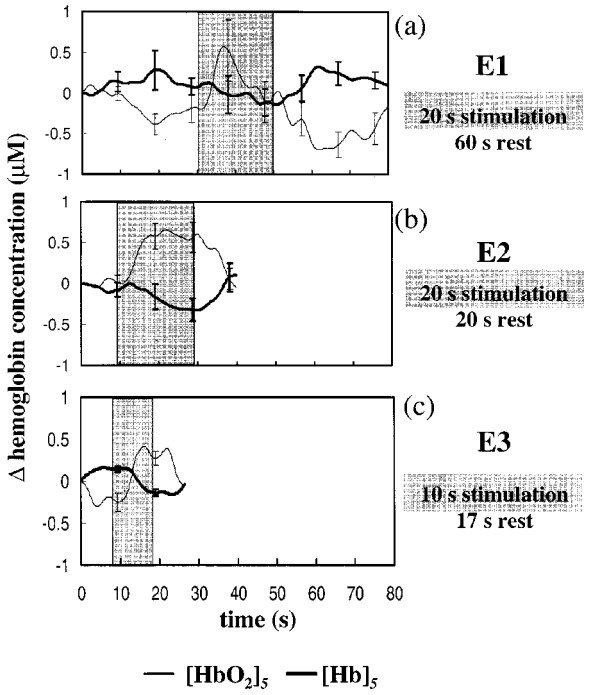


FIG. 6. Folding average of the $[\mathrm{Hb}]_5$ and $[\mathrm{HbO}_2]_5$ time traces for epochs E1 (a), E2 (b), and E3 (c). Stimulation periods are indicated by the shaded areas. The error bars represent standard errors estimated assuming normality of the distribution.

6(b), 6(c), respectively]. Stimulation periods are indicated by the shaded areas. The vertical error bars represent standard errors calculated assuming normality of the distribution of values of the $[\mathrm{Hb}]_5$ and $[\mathrm{HbO}_2]_5$ changes corresponding to the same time passed from the beginning of a stimulation/relaxation cycle. One can see that for all epochs $[\mathrm{Hb}]_5$ exhibits a decrease during stimulation, while $[\mathrm{HbO}_2]_5$ shows an increase. However, for different epochs the differences between the maximum and minimum values of the folding average changes and the corresponding standard errors are significantly different. Unlike epochs E2 and E3, during epoch E1 only the oxy-hemoglobin concentration variation between the stimulation and relaxation exceeds the standard error, while in the deoxy-hemoglobin signal all error bars significantly overlap. One should note, however, that since the number of samples for each epoch is small, the normality

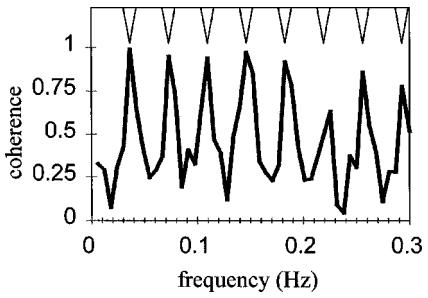


FIG. 7. Spectrum of coherence between the $[\mathrm{Hb}]_5$ signal and the stimulation wave for epoch E3. The wedge-shaped markers indicate the harmonics of the stimulation repetition frequency.

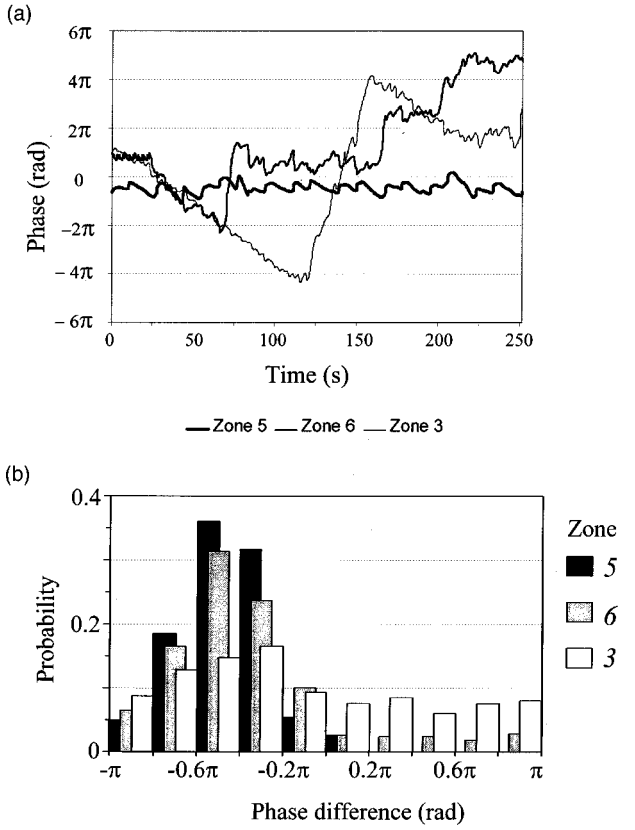


FIG. 8. (a) Time evolutions of the differences of phases of analytical signals corresponding to $[\mathrm{Hb}]_3$, $[\mathrm{Hb}]_5$, $[\mathrm{Hb}]_6$ and the stimulation wave during epoch E3; (b) statistical distributions of the phase differences of $[\mathrm{Hb}]_3$ and stimulation wave, $[\mathrm{Hb}]_5$ and stimulation wave, and $[\mathrm{Hb}]_6$ and stimulation wave, restricted to the interval $(-\pi, \pi)$. Three overlapping bars of different gray densities show probability values for $[\mathrm{Hb}]_3$, $[\mathrm{Hb}]_5$, and $[\mathrm{Hb}]_6$ corresponding to each of the ten bins covering the interval $(-\pi, \pi)$.

of the distribution may not be tested with a high significance. Therefore, the error bars in Fig. 6 rather give an idea about the variability of the values than show the standard errors associated with a normal distribution. Note that the $[\mathrm{HbO}_2]_5$ folding average trace in Fig. 6(a) has two minima: one is before the stimulation period, and another is after it. This is in agreement with the fact that the $[\mathrm{HbO}_2]_5$ power spectrum in Fig. 3(b) has the highest peak at the second harmonic of the stimulation repetition frequency.

In Fig. 7 the spectrum of coherence between the $[\mathrm{Hb}]_5$ signal and the stimulation wave is shown for the epoch E3. One can see that the coherence is close to one for the fundamental stimulation frequency and for a number of harmonics up to the fourth one, which demonstrates a high coherence of the $[\mathrm{Hb}]_5$ signal with the stimulation during epoch E3.

### C. Phase synchronization analysis

The power spectra presented in Sec. III B reveal frequency locking of the [Hb] and $[\mathrm{HbO}_2]$ time series with stimulation. Since the frequency locking may be an indication of phase synchronization, we calculated the corresponding PSIs. Figure 8(a) shows the time evolutions of the phase

TABLE I. Detected types of phases synchronization between the stimulation wave and oxy- (deoxy-) hemoglobin signals and corresponding PSI values. The estimated lower limit of PSI corresponding to significant phase synchronization is 0.07. In the cases when PSIs are below this limit, the type of phase synchronization assumed to obtain a given PSI value is shown in parentheses.

| | | Zone *1* | | Zone *2* | | Zone *3* | | Zone *4* | | Zone *5* | | Zone *6* | |
|---|---|---|---|---|---|---|---|---|---|---|---|---|---|
| Epoch | | Oxy | Deoxy | Oxy | Deoxy | Oxy | Deoxy | Oxy | Deoxy | Oxy | Deoxy | Oxy | Deoxy |
| E1 | Type | 2:1 | None (2:1) | None (2:1) | None (2:1) | None (2:1) | None (2:1) | 2:1 | None (2:1) | 2:1 | None (2:1) | 2:1 | None (2:1) |
| | PSI | 0.14 | 0.03 | 0.05 | 0.01 | 0.06 | 0.02 | 0.09 | 0.01 | 0.23 | 0.06 | 0.14 | 0.03 |
| E2 | Type | 1:1 | None (1:1) | None (1:1) | None (1:1) | None (1:1) | None (1:1) | None (1:1) | None (1:1) | 1:1 | 1:1 | 1:1 | 1:1 |
| | PSI | 0.08 | 0.05 | 0.01 | 0.03 | 0.02 | 0.03 | 0.01 | 0.06 | 0.21 | 0.24 | 0.07 | 0.13 |
| E3 | Type | None (1:1) | None (1:1) | None (1:1) | None (1:1) | None (1:1) | None (1:1) | None (1:1) | None (1:1) | 1:1 | 1:1 | 1:1 | 1:1 |
| | PSI | 0.05 | 0.05 | 0.01 | 0.05 | 0.01 | 0.01 | 0.02 | 0.03 | 0.20 | 0.44 | 0.16 | 0.24 |

differences of the analytical signals corresponding to the stimulation and hemoglobin response during epoch E3. One can see that the phase difference between $[\mathrm{Hb}]_5$ and stimulation always oscillates around some average level, and the deviations from this level never exceed $2\pi$. Physically, this means that the stimulation and the response are always in phase within the noise. On the contrary, the curve representing the phase difference of the stimulation and $[\mathrm{Hb}]_6$ during E3 exhibits a number of horizontal plateaus broken by the phase jumps. Note that the magnitude of each jump is close to an integer multiple of $2\pi$. Therefore, when the relative phase is reduced to the interval $(-\pi, \pi)$, the horizontal plateaus are approximately at the same level. The phase of the analytical signal corresponding to $[\mathrm{Hb}]_3$ does not exhibit any plateaus.

The histograms in Figs. 8(b) represent the statistical distributions of the phase differences reduced to the interval $(-\pi, \pi)$. In terms of these histograms, the ''strength'' of the phase synchronization is determined by the sharpness of the distribution. One can see that the distribution corresponding to $[\mathrm{Hb}]_5$ is sharper than that for $[\mathrm{Hb}]_6$, which has a nonzero probability over the whole range $(-\pi, \pi)$. The distribution for $[\mathrm{Hb}]_3$ is almost homogeneous. It is the phase histogram sharpness that is quantified by the PSI (see the definition in Sec. II F) to measure the phase synchronization ''strength.''

Table I summarizes the results of the analysis of phase synchronization between the stimulation wave and hemoglobin signals during epochs E1, E2, and E3. One can see that during epochs E2 and E3 some zones exhibit (1:1) phase synchronization in $[\mathrm{HbO}_2]$, [Hb], or in both signals. Unlike E2 and E3, during epoch E1 some zones exhibit (2:1) synchronization in $[\mathrm{HbO}_2]$, which is in agreement with Fig. 6(a), showing two maxima of the oxy-hemoglobin change during the stimulation/relaxation period, and with Fig. 3(b) displaying the highest $[\mathrm{HbO}_2]_5$ power spectrum peak at the second harmonic of stimulation repetition frequency. However, during E1 none of the zones shows significant phase synchronization in the [Hb] signal.

## IV. SPATIAL MAPPING OF BRAIN ACTIVITY

### A. Optical maps obtained from folding average, spectral, and phase synchronization analysis

As described in Sec. II H, square pixels in the coordinate grid of optical maps correspond to six zones in the motor cortex area. Figure 9 represents the optical maps of the brain response to the stimulation during epochs E1, E2, and E3 in

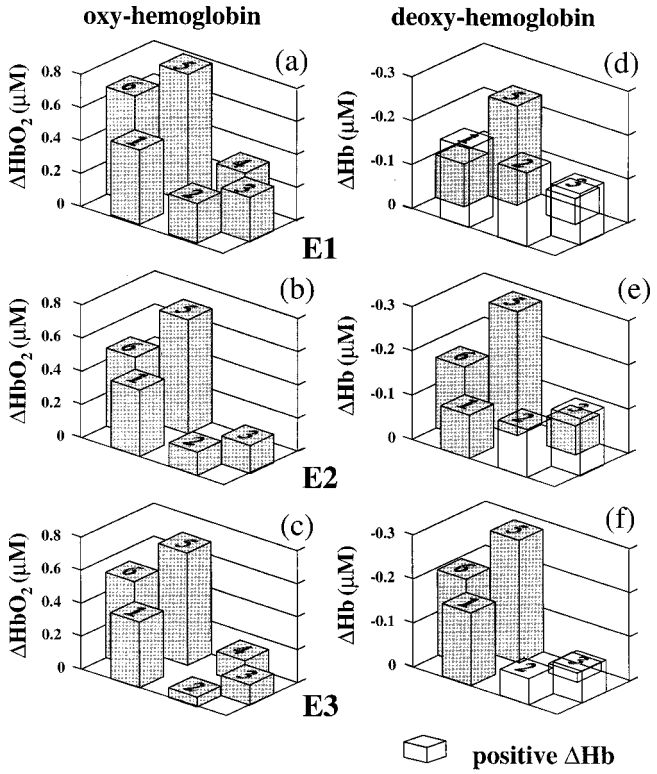


FIG. 9. Spatial maps of the brain signals during epochs E1, E2, and E3 in terms of the magnitude of the folding-average changes of $[\mathrm{HbO}_2]$ (a)–(c) and [Hb] (d)–(f) from relaxation to stimulation conditions. Note that since the deoxy-hemoglobin ''response'' corresponds to the negative concentration change from the relaxation to the stimulation, the vertical axis in (d)–(f) shows negative values. The clear bars in (d)–(f) indicate reversed positive values of the average [Hb] change.

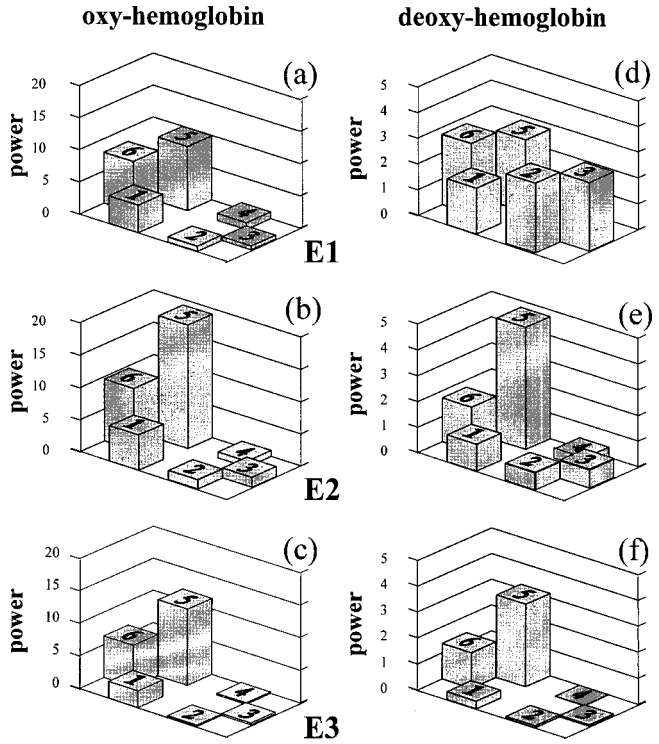


FIG. 10. Spatial maps of brain oxy- and deoxy-hemoglobin signals during epochs E1, E2, and E3 in terms of the power spectra of $[HbO_2]$ (a)–(c) and [Hb] (d)–(f) power spectra. The plotted value is the power spectrum magnitude at the second harmonic of the stimulation wave frequency [(a) and (d)], and at the fundamental frequency of the stimulation wave [(b), (c), (e), and (f)].

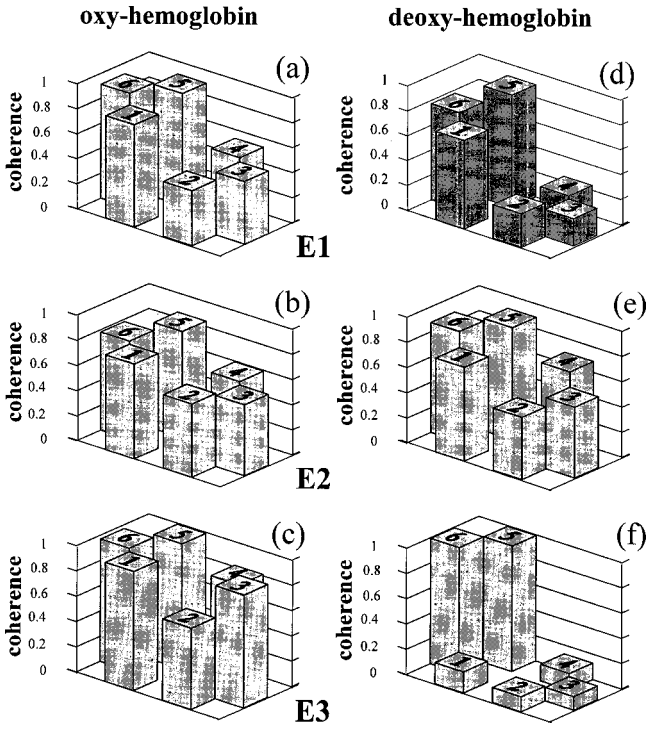


FIG. 11. Spatial maps of brain oxy- and deoxy-hemoglobin signals during epochs E1, E2, and E3 in terms of the $[HbO_2]$ (a)–(c) and [Hb] (d)–(f) spectrum of coherence with the stimulation wave. The plotted value is the coherence magnitude at the second harmonic of the stimulation wave frequency [(a) and (d)], and at the fundamental frequency of the stimulation wave [(b), (c), (e), and (f)].

terms of the $[HbO_2]$ [Figs. 9(a)–9(c)] and [Hb] [Figs. 9(d)–9(f)] magnitude of folding-average changes from stimulation to relaxation, defined in Sec. II E. Note that unlike the oxy-hemoglobin response, the deoxy-hemoglobin response corresponds to the negative concentration change from the relaxation to the stimulation.

Figure 10 shows maps of brain oxy- and deoxy-hemoglobin signals during epochs E1, E2, and E3 in terms of the $[HbO_2]$ [Figs. 10(a)–10(c)] and [Hb] [Figs. 10(d)–10(f)] power spectra. Maps in Fig. 11 display spatial distributions of coherence between the stimulation wave and fluctuations in $[HbO_2]$ [Figs. 11(a)–11(c)] and [Hb] [Figs. 11(d)–11(f)]. The bar heights in Figs. 10 and 11 [except for Figs. 10(a) and 10(d), and 11(a) and 11(d)] correspond to the power spectrum and coherence magnitudes, respectively, at the stimulation repetition frequency. Note that since during epoch E1 oxy- and deoxy-hemoglobin concentrations exhibit response at the second harmonic of the stimulation repetition frequency, maps in Figs. 10(a) and 10(d), and 11(a) and 11(d), show power spectrum and coherence values at the second harmonic. Comparing power spectrum maps for the oxy- and deoxy-hemoglobin signals, one should take into account that the vertical scale of power spectrum maps for oxy-hemoglobin [Figs. 10(a)–10(c)] is four times larger than that for deoxy-hemoglobin [Figs. 10(d)–10(f)].

The maps of the PSI spatial distribution for the oxy- and deoxy-hemoglobin signals during epochs E1–E3 are presented in Figs. 12(a)–12(c), and Figs. 12(d)–12(f), respectively (see also Table I). The zones showing no statistically significant phase synchronization are labeled with clear bars. Note that the PSI values plotted in Figs. 12(a) and 12(d) correspond to the (2:1)-phase synchronization. As it was discussed in Sec. III C, during E1, no statistically significant synchronization of any $(n:m)$ type was detected in any of the [Hb] signals [Fig. 12(d)]. Since during E1 the power spectra of $[Hb]_1$, $[Hb]_5$, and $[Hb]_6$ signals indicate their (2:1) frequency synchronization with the stimulation wave, Fig. 12(d) represents the PSI values obtained assuming the (2:1)—phase synchronization.

### B. Comparison of the optical maps: Oxy-hemoglobin

The maps displaying oxy-hemoglobin signals in terms of the folding average change of magnitude [Figs. 9(a)–9(c)], the power spectrum magnitudes [Figs. 10(a)–10(c)], and the phase synchronization index [Figs. 12(a)–12(c)] show similar spatial patterns for all three exercise epochs. The response is always localized in adjacent zones *1*, *4*, *5*, and *6*. The folding average and PSI maps show some narrowing of the $[HbO_2]$ response area with the increase of the stimulation frequency. Spatial patterns of $[HbO_2]$ coherence with the stimulation [Figs. 11(a)–11(c)] for the three epochs are also similar, but they reveal no localization unlike the folding

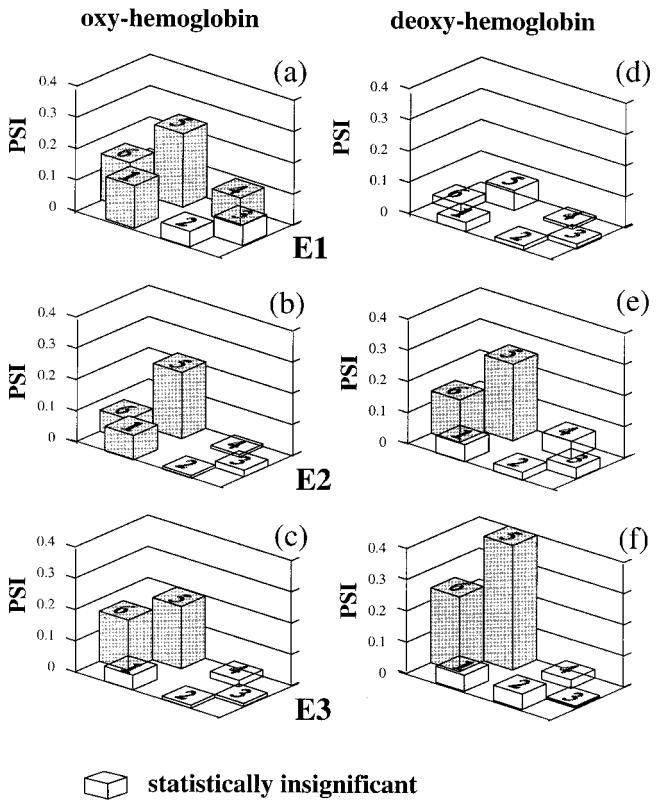


FIG. 12. Spatial maps of brain oxy- and deoxy-hemoglobin signals during epochs E1, E2, and E3 in terms of the $[HbO_2]$ (a)–(c) and [Hb] (d)–(f) index of phase synchronization with the stimulation wave. The plotted value is PSI for the 2:1 type of synchronization [(a) and (d)], and 1:1 type of synchronization (b), (c), (e), and (f).

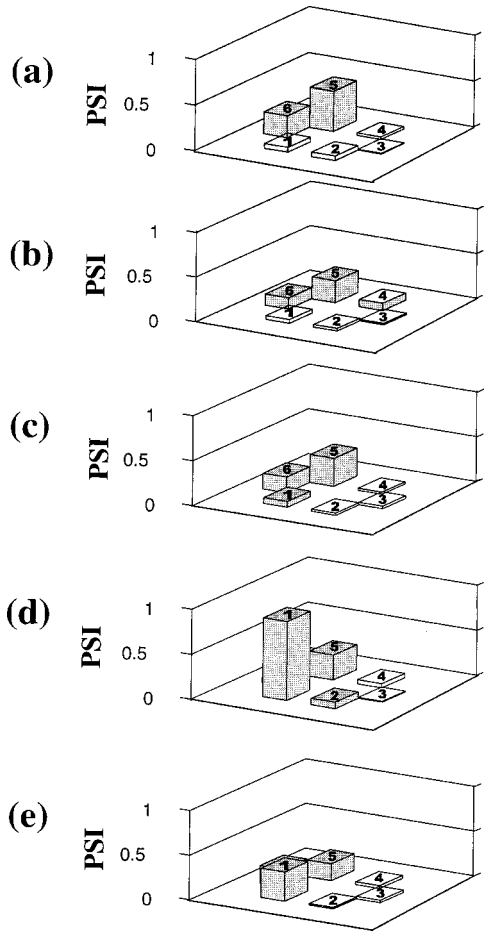


FIG. 13. Deoxy-hemoglobin PSI maps for five different subjects (a)–(e) obtained under conditions of epoch E3 (10/17 s stimulation/relaxation period).

average, power spectrum, and phase synchronization patterns. This demonstrates a qualitative difference between the PSI and coherence, stressed in Ref. 19.

### C. Comparison of the optical maps: Deoxy-hemoglobin

#### *1. Epoch E1*

The power-spectrum map [Fig. 10(d)] shows fluctuations in the entire region. The [Hb] fluctuations at zones *1*, *5*, and *6* are coherent with the stimulation wave [Fig. 11(d)]. There is no phase synchronization between the [Hb] signal and stimulation wave in any zone [Fig. 12(d)]. Although the folding-average map [Fig. 9(d)] shows signals in zones 5 and 6, the variability in values plotted in this map is high [see error bars in Fig. 6(a)].

#### *2. Epoch E2*

The folding average [Fig. 9(e)], power spectrum [Fig. 10(e)], and phase synchronization [Fig. 12(e)] maps indicate response localization in zones *5* and *6*. However, coherence between the signal and the stimulation wave [Fig. 11(e)] is high in the entire region, which is similar to the $[HbO_2]$ coherence distribution during the same exercise.

#### *3. Epoch E3*

All maps [Figs. 9(f), 10(f), 11(f), and 12(f)] show signal localization in zones 5 and 6. The similarity of the coherence map [Fig. 11(f)] with the other maps showing the [Hb] response during epoch E3 is due to a low amplitude of fluctuations in zones *1–4* compared to zones *5–6* [see also Fig. 10(e)].

## V. INTERSUBJECT VARIABILITY

The data from the 43-year-old male presented above demonstrate a number of features common for most members of the group of five male subjects. Namely, for all stimulation frequencies, optical maps of the [Hb] signals represent narrower response areas than the maps of $[HbO_2]$ signals. The localization of the [Hb] response is particularly significant when the response is quantified by the phase synchronization index or magnitude of folding average changes. Unlike oxy-hemoglobin, the PSI values of deoxy-hemoglobin signals in the zone of synchronization exhibit a strong dependence on the stimulation frequency, and typically increase with the frequency increase. Figure 13 shows the deoxy-hemoglobin PSI maps for five different subjects obtained under conditions of epoch E3 (10/17 s stimulation/relaxation period).

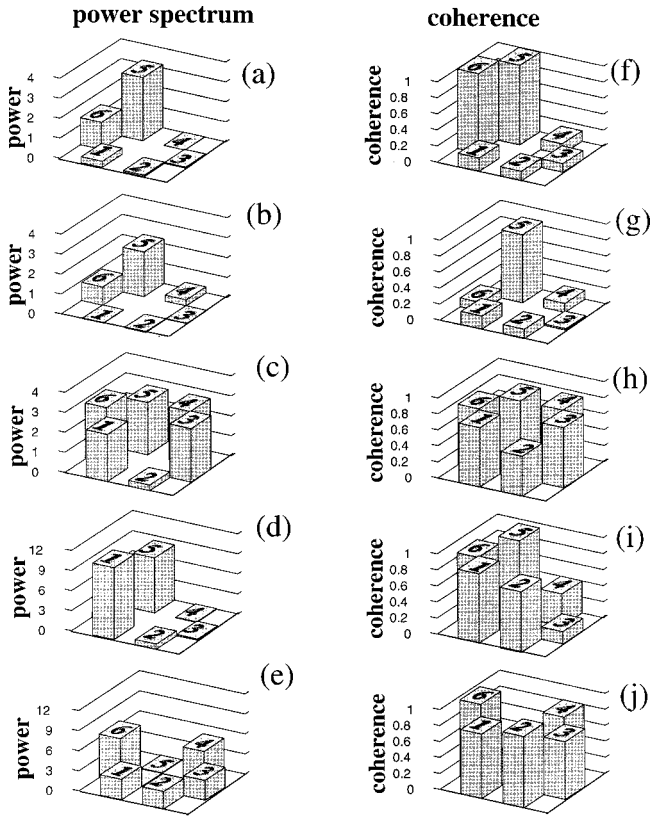


FIG. 14. Deoxy-hemoglobin power spectrum maps (a)–(e) and coherence maps (f)–(g) for the same subjects and same conditions as in Fig. 13.

One can see that for all subjects the center of the zone of synchronization appears in the precentral part of the probed area close to the central line. Another common observation is that at highly synchronized states of the [Hb] signal its power spectrum exhibits a narrow peak near the stimulation frequency, but there is no significant difference between the power spectrum magnitudes at this frequency observed at rest and stimulation conditions.

Figures 5(d), 10(c), and 10(f) show a general decrease of the hemoglobin fluctuations outside of the localized area, where hemodynamic changes are highly synchronized with the stimulation. Such a suppression of fluctuations was not found in all subjects. Although all subjects demonstrated signal localization in terms of its phase synchronization with stimulation, in some subjects fluctuations outside the area of synchronization continued during all epochs. Figure 14 shows [Hb] power spectra and coherence maps for the same five subjects and the same exercise conditions as Fig. 13. One can see that three subjects exhibit fluctuation localization [Figs. 14(a) and 14(f), 14(b), and 14(g), and 14(d)], but two others do not [Figs. 14(c) and 14(h), 14(e) and 14(j)]. In Figs. 14(a)–14(e) one can also see that in different subjects the amplitude of hemoglobin fluctuations is considerably different. This may be due to such anatomic factors as the difference in the thickness of the CSF layer, arachnoid granulations, etc.

In some cases, the temporal and spectral properties of fluctuations outside the area of synchronization were significantly different from the rest. However, we could not derive any typical pattern of fluctuations outside the zone of synchronization. Apart from the fluctuation suppression, we observed random or regular (but not synchronous with the stimulation) changes. Figure 15 shows an example of apparently regular hemodynamic changes, both in the zone of synchronization [Fig. 15(a), zone *6*] and outside it [Fig. 15(b), zone *2*], which was observed in the 34-year-old male during the exercise epoch with a 20/20 s stimulation/relaxation period.

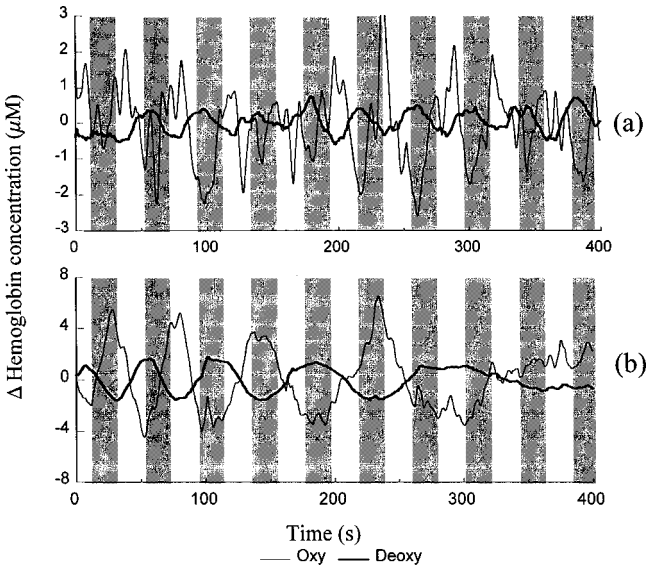


FIG. 15. $[HbO_2]$ and [Hb] time traces measured in a 34-year-old subject during an exercise epoch of a 20/20 s stimulation/relaxation period at zones *6*(a) and *2*(b). The shaded areas indicate stimulation periods.

When $[HbO_2]$ and [Hb] changes were synchronous with stimulations, we observed increases of $[HbO_2]$ and decreases of [Hb] in all members of the group but one. One member (60-year-old male) demonstrated such a ''typical'' hemodynamic pattern during only one epoch (10/10 s stimulation/relaxation period) at zones *1* and *2* [see Fig. 16(a)]. During other epochs, these and other zones showed different combinations of the [Hb] and $[HbO_2]$ changes, which were phase synchronous with the stimulation wave. Particularly during the epoch with the 20/20 s stimulation/relaxation period, both $[Hb]_1$ and $[HbO_2]_1$ exhibited prominent signals at the second harmonic of the stimulation frequency. The folding average traces for these signals show an increase in both $[HbO_2]_1$ and $[Hb]_1$ during stimulation [Fig. 16(b)].

## VI. DISCUSSION

Our fast multichannel NIRS measurements of brain activity during the repetitive motor task show that depending on the duration of stimulation and relaxation phases and on the zone in the cortex, oxy- and deoxy-hemoglobin concentrations exhibit either regular changes as the $[Hb]_5$ trace in Fig. 4(d), or fluctuations similar to those observed at rest. In the cases when the signals are irregular, the detection and characterization of the response requires mathematical techniques. Because of the complicated hemoglobin concentra-

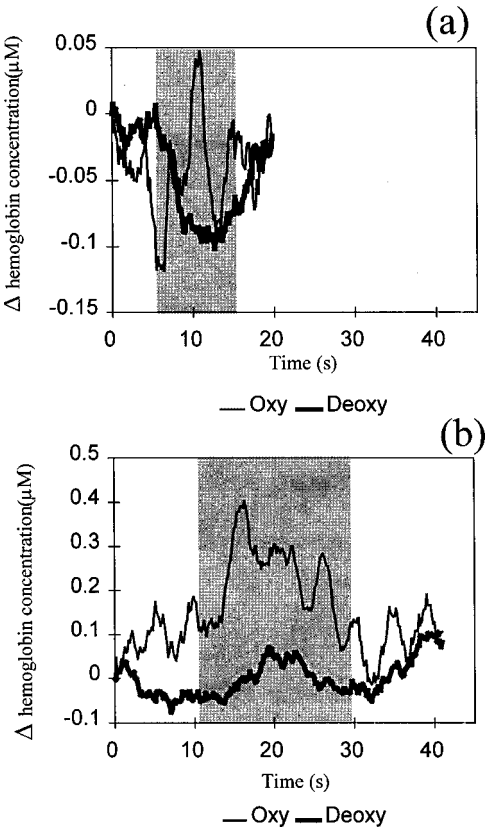


FIG. 16. Folding average traces of $[HbO_2]_l$ and $[Hb]_l$ observed in a 60-year-old subject (a) during an exercise epoch with 10/10 s stimulation/relaxation; (b) 20/20 s stimulation/relaxation. The shaded areas indicate stimulation periods.

tion changes, only the combination of different analysis methods can bring an understanding of the process. An effective tool for the brain response detection is the statistical analysis of the significance of hemodynamic changes caused by the stimulation. However, one should take into account that the typical time limits of a motor stimulation protocol result in a small number of stimulation/relaxation cycles. Therefore, the significance tests based on the assumption of any particular type of statistical distribution are not fully justified. The most robust is the sign test.[20] However, the power of this test can be low because of the small number of samples. For example, in the case of 11 decreases and 4 increases of [Hb] during 15 stimulations, the sign test reveals no significance ($P \leqslant 0.118$), while with the same proportion of positive and negative changes during 60 stimulations the significance would be very high ($P \leqslant 0.0004$). Another option is the Wilcoxon matched-pair signed-rank test.[20]

When the results of the sign test and Wilcoxon test are different, as in the case of [Hb] changes during epoch E1, other analysis techniques may help us to understand the situation. One of the most popular methods is the folding average. Ideally, the folding average procedure eliminates all the processes that are not phase synchronous with the folded time intervals. However, the limitations associated with the lack of statistical information and possible non-normality of data distributions do also apply to the folding average. Indeed, the arithmetic averaging and the standard error calculation used in the folding average technique are rigorously justified only in the case of the normal distribution of averaged values. Our analysis shows that the sampled distributions of $[HbO_2]$ and [Hb] changes are not even always symmetric. Therefore, the result of the folding average analysis cannot be used as an ultimate criterion, neither for the brain response detection nor for the assessment of the signal dynamic properties.

To assess the dynamic properties of the hemoglobin signal, it is useful to perform the power spectrum analysis. The power spectrum peaks at specific frequencies may indicate frequency synchronization. However, since the power spectrum cannot quantify the interrelationship between the stimulation and hemodynamics, the coherence and quantitative phase synchronization analyses are important. Note that the meaning of the term ''response'' is different depending on what quantity, coherence or PSI, is associated with it. As an analysis of Sec. IV shows, the phase synchronization maps always show a localized response [see Figs. 11(a)–11(c), 11(e), and 11(f)], while relatively large areas in the brain may exhibit fluctuations that are coherent with the stimulation [see Figs. 10(a)–10(c), and 10(e)]. Therefore, a combination of approaches is particularly relevant for the mapping of brain functions.

The comparison of Figs. 8 and 11 indicates that the folding average and the PSI maps for each exercise correlate. However, comparing results of folding average and phase synchronization analyses, one should take into account that a strong phase synchronization is a necessary but not sufficient condition for a high signal-to-noise ratio in the folding average pattern. Indeed, even in the case of a strong phase synchronization, the amplitude fluctuations can render the folding average pattern noisy. Therefore, considering the folding average analysis results together with the phase synchronization provides a better understanding of the hemodynamics. For example, the average $[Hb]_5$ trace in Fig. 6(b) for epoch E2 shows a slanting decrease starting approximately 3 s after the onset of the stimulation, while Fig. 6(c) displays a steep $[Hb]_5$ change beginning about 5 s after the stimulation onset. The fact that the PSI value for the $[Hb]_5$ signal during E2 is significantly lower than during E3 could signify that the leading edge of the $[Hb]_5$ curve in Fig. 6(b) is due to an averaging effect rather than due to the dynamics of the process. Indeed, comparing the deoxy-hemoglobin traces in Figs. 4(c) and 4(d), one can see that the magnitude of the changes during stimulations is similar for both E2 and E3. However, during E3 the beginning of each stimulus-induced decrease in $[Hb]_5$ trace occurs almost at the same phase of the stimulation cycle, in contrast to the random phase of response during epoch E2. Furthermore, the dynamic interpretation of the folding average traces requires wariness also because of the statistical validity limitations of folding average analysis discussed above. On the other hand, such limitations as the lack of normality or symmetry of statistical distributions do not apply to the phase synchronization analysis.

As follows from our statistical analysis of deoxy-

hemoglobin changes during epoch E1 (Sec. III B), the fast multichannel NIRS assessment of brain activity provides the following advantage for the detection of a brain response to stimulation. In the cases when hemodynamic changes are small, one can improve the sensitivity by subtracting the background fluctuations observed at remote brain zones from the signals observed at stimulated area, and by combining data from separate zones in the stimulated area.

Using the light channels with short source–detector distances [5 mm; see Fig. 1(b)] we were able to compare the brain hemodynamics with that in superficial head tissue. We have found that the coherence between the short-distance (5 mm) and long-distance (28 and 40 mm) signals is low in the entire frequency band below 3.5 Hz, except for the heartbeat and respiratory frequencies. This confirms that in the long-distance signal the intracranial tissue contributions dominate over the superficial hemodynamics.

Our temporal analysis and mapping of cerebral hemodynamics reveals the following features common for the group of five subjects. Significant hemodynamic fluctuations in the brain occur not only during exercises, but also at rest. Repetitive motor stimulations lead to the appearance of the area in the cortex where the fluctuations are synchronized with the stimulation wave. The degree of synchronization quantified by PSI depends on the frequency of the stimulation wave. The changes in the degree of synchronization are more significant for the deoxy-hemoglobin signal than for the oxy-hemoglobin one. In agreement with the result of Ref. 9, our PSI maps show the uprising of the center of the synchronization area close to the central line in the precentral part of the motor cortex.

The importance of the issue of synchronization has been extensively discussed for nonlinear systems, including biological systems.[19,29] We would like to point out that there are indications, including some of our results, that functional cerebral hemodynamics can also be considered as a nonlinear synchronization phenomenon. Indeed, chaotic hemodynamic fluctuations at rest may result from the nonlinear neurovascular coupling. Such fluctuations were also reported by other researchers.[30,31] Existing mathematical models attribute the low-frequency (below 0.1 Hz) systemic spontaneous fluctuations in the blood flow for the action of the autoregulatory system intended to maintain a proper average level of arterial pressure, blood oxygenation, and other physiological parameters.[32,33] Since these models are nonlinear, they allow dynamic patterns in the form of complex nonperiodical self-sustained oscillations. One can assume that to enhance the cerebral circulation autocontrol, apart from the systemic autoregulation mechanisms, there also exists a local regulation, which is responsible for the local hemodynamic underlying fluctuations. Furthermore, if one considers the repetitive sequence of stimulations as the periodic external force acting on the nonlinear neurovascular system, depending on the frequency of the stimulation wave and subject's individuality, one can expect hemodynamic outputs associated with quantitatively and qualitatively different synchronization states. The examples of the quantitatively different synchronization states are given by the maps in Figs. 11(d)–11(f), showing different PSI values for deoxy-hemoglobin signals in the zone of synchronization. The examples of quantitatively different states are the first and second harmonic hemodynamic signals at different exercise epochs, which we observed in two subjects, and the increase or decrease of deoxy-hemoglobin concentration during stimulation at different exercise epochs observed in one subject [compare Figs. 12(a) and 12(b)].

One should note that the synchronization of the underlying fluctuations with the stimulation together with the use of the folding averaging procedure for data analysis can lead to the invalid conclusion that the oxygenation changes due to stimulations are much larger than fluctuations at rest conditions. We believe that further study of the underlying cerebral hemodynamic fluctuations and the understanding of their role in the dynamics under stimulation conditions is important to answer the question why the measurements of brain hemodynamics during stimulations show the tremendous local oxygen consumption increase, which is disproportional with the actual oxygen need.[34]

There are also indications of the possible importance of local hemodynamics phase and frequency synchronization with the systemic rhythms (such as the heartbeat and respiration) for brain response formation. Note that in Fig. 3(d) the respiratory peak in the $[\mathrm{Hb}]_5$ power spectrum coincides with the fourth harmonic of the stimulation repetition frequency, i.e., there is a (4:1) frequency synchronization between the ''respiratory'' wave and the stimulation. [However, the PSI estimation did not reveal statistically significant phase synchronization, although the mean slope of the relative phase $\Psi_{41}(t)$ is equal to zero, in agreement with the (4:1)-type frequency locking.] Using the quantitative phase synchronization analysis, we also detected a high degree of phase locking between the pulse and stimulation wave [for example, during epoch E3, PSI for (31:1), pulse-stimulation synchronization is equal to 0.67].

## VII. CONCLUSION

Using multichannel near-infrared cerebral spectroscopy we have found that the hemoglobin changes in the motor cortex under periodic motor stimulation can be highly regular or irregular, depending on the duration of the stimulation/relaxation period. We have shown that in the case of complex hemodynamics, the response to stimulations can be detected combining statistical, folding average, power spectrum, coherence, and quantitative phase synchronization analyses. Using these techniques, we revealed differences in the oxy- and deoxy-hemoglobin dynamics during periodic motor stimulation. We found that the oxy-hemoglobin concentration changes are significant and phase synchronous with the stimulation at most of the exercise conditions. The deoxy-hemoglobin response to stimulations depends on the stimulation and relaxation timing, partially due to the interference with the background fluctuations, and partially due to the possible stimulation–response phase synchronism. Using the power spectrum, coherence and phase synchronization

analysis, we have shown that functional stimulation can cause local frequency and phase synchronization of cerebral hemodynamic fluctuations.

We obtained maps showing oxy- and deoxy-hemoglobin dynamics in terms of folding average changes, power spectrum, coherence, and phase synchronization with the periodic stimulation wave. We have shown that while a relatively large area of the brain may exhibit fluctuations that are coherent with the stimulation wave, when phase synchronization occurs, the phase synchronization maps always show a localized response of the deoxy-hemoglobin signal. Our preliminary conclusion is that the regularity and localization of the hemodynamic response to the periodical motor stimulation might be higher when systemic rhythms, such as the heartbeat and breathing, are phase or frequency locked with the stimulation wave.

## ACKNOWLEDGMENTS

This work was supported by National Institutes of Health (NIH) Grant No. CA57032, and Whitaker-NIH Grant No. RR10966.

[a]Electronic mail: toronov@uiuc.edu
[b]Current address: Bioengineering Center, Department of Electrical Engineering and Computer Science, Tufts University, 4 Colby Street, Medford, Massachusetts 02155-6013.

[1] A. Villringer and B. Chance, ''Non-invasive optical spectroscopy and imaging of human brain function,'' Trends Neurosci. **20**, 435–442 (1997).
[2] R. Wenzel, H. Obrig, J. Ruben, K. Villringer, A. Thiel, J. Bernarding, U. Dirnagl, and A. Villringer, ''Cerebral blood oxygenation changes induced by visual stimulation in humans,'' J. Biomed. Opt. **1**, 399–404 (1996).
[3] J. H. Meek, M. Firbank, C. E. Elwell, J. Atkinson, O. Braddick, and J. S. Wyatt, ''Regional hemodynamic responses to visual stimulation in awake infants,'' Pediatr. Res. **43**, 840–843 (1998).
[4] T. Kato, A. Kamei, S. Takashima, and T. Ozaki, ''Human visual cortical function during photic stimulation monitoring by means of near-infrared spectroscopy,'' J. Cereb. Blood Flow Metab. **13**, 516–520 (1993).
[5] C. Hirth, H. Obrig, J. Valdueza, U. Dirnagl, and A. Villringer, ''Simultaneous assessment of cerebral oxygenation and hemodynamics during a motor task,'' Adv. Exp. Med. Biol. **411**, 461–469 (1997).
[6] A. M. Gorbach, ''Infrared imaging of brain function,'' Adv. Exp. Med. Biol. **333**, 95–123 (1993).
[7] C. Hirth, K. Villringer, A. Thiel, J. Bernarding, W. Muhlnickl, H. Obrig, U. Dirnagl, and A. Villringer, ''Towards brain mapping combining near-infrared spectroscopy and high resolution 3D MRI,'' Adv. Exp. Med. Biol. **413**, 139–147 (1997).
[8] A. Maki, Y. Yamashita, Y. Ito, E. Watanabe, Y. Mayanagi, and H. Koizumi, ''Spatial and temporal analysis of human motor activity using noninvasive NIR topography,'' Med. Phys. **22**, 1997–2005 (1995).
[9] E. Watanabe, Y. Yamashita, A. Maki, Y. Ito, and H. Koizumi, ''Non-invasive functional mapping with multi-channel near infra-red spectroscopic topography in humans,'' Neurosci. Lett. **205**, 41–44 (1996).
[10] H. Obrig, C. Hirth, J. G. Junge-Hulsing, C. Doge, R. Wenzel, T. Wolf, U. Dirnagl, and A. Villringer, ''Length of resting period between stimulation cycles modulates hemodynamic response to a motor stimulus,'' Adv. Exp. Med. Biol. **411**, 471–480 (1997).
[11] M.-P. Deiber, R. E. Passingham, J. G. Colebatch, K. J. Friston, P. D. Nixon, and R. S. J. Frackowiak, ''Cortical areas and the selection of movement: a study with positron emission tomography,'' Exp. Brain Res. **84**, 393–402 (1991).
[12] S.-G. Kim, J. Ashe, K. Hendrick, J. M. Ellermann, H. Merkle, K. Ugurbil, and A. P. Georgopulos, ''Functional magnetic resonance imaging of motor cortex: hemispheric asymmetry and bandedness,'' Science **261**, 613–617 (1993).
[13] Y. Hoshi and M. Tamura, ''Fluctuations in the cerebral oxygenation state during the resting period in functional mapping studies of the human brain,'' Med. Biol. Eng. Comput. **35**, 328–330 (1997).
[14] B. Chance, E. Anday, S. Nioka, S. Zhou, L. Hong, K. Worden, C. Li, T. Murray, Y. Ovetsky, D. Pidikiti, and R. Thomas, ''A novel method for fast imaging of brain function, non-invasively, with light,'' Opt. Express **2**, 411–423 (1998).
[15] R. M. Danen, Y. Wang, X. D. Li, W. S. Thayer, and A. G. Yodh, ''Regional imager for low-resolution functional imaging of the brain with diffusing near-infrared light,'' Photochem. Photobiol. **67**, 33–40 (1998).
[16] T. Tamura, H. Eda, M. Takada, and T. Kubodera, ''New instrument for monitoring hemoglobin oxygenation,'' Adv. Exp. Med. Biol. **248**, 103–107 (1989).
[17] M. Tamura, Y. Hoshi, and F. Okada, ''Localized near-infrared spectroscopy and functional optical imaging of brain activity,'' Philos. Trans. R. Soc. London, Ser. B **352**, 737–742 (1997).
[18] J. S. Bendat and A. G. Piersol, *Random Data: Analysis and Measurement Procedures* (Wiley, New York, 1986).
[19] P. Tass, M. G. Rosenblum, J. Weule, J. Kurths, A. Pikovsky, J. Volkmann, A. Schnitzler, and H.-J. Freund, ''Detection of *n:m* phase locking from noisy data: Application to magnetoencephalography,'' Phys. Rev. Lett. **81**, 3291–3294 (1998).
[20] G. K. Kanji, *100 Statistical Tests* (Sage publications, London, 1993).
[21] H. H. Jasper, ''Report of the committee on methods of clinical examination in electroencephalography,'' Electroencephalogr. Clin. Neurophysiol. **10**, 370–375 (1957).
[22] A. Ishimaru, ''Diffusion of light in turbid material,'' Appl. Opt. **28**, 2210–2215 (1989).
[23] A. Duncan, J. H. Meek, M. Clemence, C. E. Elwell, L. Tyszczuk, M. Cope, and D. T. Delpy, ''Optical pathlength measurements on adult head, calf and forearm and the head of the newborn infant using phase resolved optical spectroscopy,'' Phys. Med. Biol. **40**, 295–304 (1995).
[24] S. Fantini *et al.*, ''Frequency-domain multichannel optical detector for noninvasive tissue spectroscopy and oximetry,'' Opt. Eng. (Bellingham) **34**, 32–42 (1995).
[25] S. Wray, M. Cope, D. T. Delpy, J. S. Wyatt, and E. O. Reynolds, ''Characterization of the near infrared absorption spectra of cytochrome aa3 and haemoglobin for the non-invasive monitoring of cerebral oxygenation,'' Biochim. Biophys. Acta **933**, 184–192 (1988).
[26] E. Okada, M. Firbank, M. Shweiger, S. Arridge, M. Cope, and D. Delpy, ''Theoretical and experimental investigation of near-infrared light propagation in a model of the adult head,'' Appl. Opt. **36**, 21–31 (1997).
[27] R. W. Hamming, *Digital Filters* (Prentice–Hall, Englewood Cliffs, NJ, 1977).
[28] C. E. Elwell, H. Owen-Reece, J. C. Wyatt, M. Cope, E. O. Reynolds, and D. T. Delpy, ''Influence of respiration and changes in expiratory pressure on cerebral haemoglobin concentration measured by near infrared spectroscopy,'' J. Cereb. Blood Flow Metab. **16**, 353–357 (1996).
[29] K. Niizeki and Y. Miyamoto, ''Cardiolocomotor interactions during dynamic handgrip and knee extension exercises. Phase-locked synchronization and its physiological implications,'' Adv. Exp. Med. Biol. **450**, 199–206 (1998).
[30] J. E. Mayhew, S. Askew, Y. Zheng, J. Porrill, G. W. Westby, P. Redgrave, D. M. Rector, and R. M. Harper, ''Cerebral vasomotion: a 0.1-Hz oscillation in reflected light imaging of neural activity,'' Neuroimage **4**, 183–193 (1996).
[31] A. G. Hudetz, R. J. Roman, and D. R. Harder, ''Spontaneous flow oscillations in the cerebral cortex during acute changes in mean arterial pressure,'' J. Cereb. Blood Flow Metab. **12**, 491–499 (1992).
[32] J. B. Madwed, P. Albrecht, R. G. Mark, and R. J. Cohen, ''Low-frequency oscillations in arterial pressure and heart rate: a simple computer model,'' Am. J. Physiol. **256**, H1573–H1579 (1989).
[33] C. D. Wagner, and P. B. Persson, ''Chaos in the cardiovascular system: an update,'' Cardiovasc. Res. **40**, 257–264 (1998).
[34] A. G. Hudetz, ''Mathematical model of oxygen transport in the cerebral cortex,'' Brain Res. **817**, 75–83 (1999).